Catalysis Science & Technology

ROYAL SOCIETY OF CHEMISTRY

PAPER

View Article Online
View Journal | View Issue

Cite this: *Catal. Sci. Technol.*, 2025, **15**, 114

On the mechanisms of ethane dehydrogenation on silica-supported mononuclear Fe†

Sakshi Satyanand, [a] Sanjana Srinivas, [a] Dionisios G. Vlachos *[abc] and Stavros Caratzoulas[bc]

With the increasing interest in developing catalytic materials based on atomically dispersed transition metals on heterogeneous supports, it is necessary to have an atomic-level understanding of the factors that impact their structural and electronic properties and, ultimately, their reactivity. In this contribution, we address and elucidate with electronic structure calculations open questions related to the ethane dehydrogenation mechanism on silica-supported mononuclear Fe(II) and Fe(III) sites. Contrary to prior hypotheses, we determine that the σ-metathesis on Fe(II) sites is an unlikely dehydrogenation mechanism. On tricoordinate and tetracoordinate Fe(II)@SiO_2, the reaction proceeds via heterolytic C–H bond activation and β-hydride elimination facilitated by spin-crossing. Atomically dispersed Fe(III) grafted on SiO_2 exhibits a more complex behavior as it seems to be undergoing autoreduction and we propose a new redox ethane dehydrogenation mechanism which, remarkably, is energetically competitive with the heterolytic C–H activation mechanism previously identified for other transition metals.

Received 19th September 2024,
Accepted 26th November 2024

DOI: 10.1039/d4cy01118j

rsc.li/catalysis

1. Introduction

Transforming hydrocarbons through C–H bond activation is a pivotal challenge in chemistry as it offers us access to molecules of economic importance. Dehydrogenation of ethane to ethylene is garnering renewed interest on account of the abundant shale gas.[1,2] In tandem, sustainability efforts are driving the need for catalytic materials utilizing earth-abundant metals.[3] Operating at the single atom limit further allows us to leverage atom efficiency and ease of separation.[4]

Amorphous silica-supported mononuclear first row 3*d*-metals M@SiO_2 (M = Fe(II),[5] Co(II)[6–8] and Zn(II)[9]) have shown promising catalytic activity for ethane dehydrogenation, with Co(II) demonstrating high selectivity. The mechanism on Co(II)@SiO_2 has been elucidated by Srinivas *et al.*,[10] who showed that high-spin (quartet) Co d^7 catalyzes the C–H activation heterolytically and that the ensuing β-H elimination is facilitated by spin-crossing to the doublet state. By microkinetics simulations, Srinivas *et al.*[10] further showed that the β-H elimination is rate-controlling.

Isolated Fe species grafted on silica or incorporated in the framework of silicates also exhibit interesting catalytic properties. Hu *et al.*[5] synthesized isolated 3-coordinate Fe(II)@SiO_2 and demonstrated that it was selective and stable for propane dehydrogenation. The mechanism in this case has not been elucidated, although it has been suggested that the reaction could proceed either via the heterolytic pathway described above or via σ-bond metathesis between the Fe-hydride and an alkane molecule, to form H_2 and an Fe-alkyl as in the case of late transition metal complexes.[11,12] Isolated Fe(III) species have been incorporated in the matrix of SBA-15 by Nozaki *et al.*[13] and by Cheng *et al.*[14] Site stability of Fe(III) on amorphous silica is challenging due to mobile Fe centers that form FeO_x agglomerates, which can be mitigated by deploying bulky ligands as precursors.[13,15] Grosso-Giordano *et al.*[15] have further hypothesized that the crystalline spatial arrangement of hydroxyls in siliceous zeolites provides a more favorable environment for enhanced Fe(III) uptake compared to amorphous silica in grafting experiments.[15] Interestingly, Lobo and co-workers have suggested a redox mechanism for the dehydrogenation of propane over isomorphously substituted H–[Fe(III)]-ZSM5 (ref. 16 and 17) but to the best of our knowledge the mechanism has not been confirmed. Notably, d^4 to d^8 metal centers can cleave C–H bonds through various pathways.[18]

Tuning the coordination environment of surface-bound, well-defined transition metals is critical to the development of new catalysts for C–H activation on heterogeneous supports with well-defined catalyst species. In the case of

[a] *Department of Chemical and Biomolecular Engineering, University of Delaware, 150 Academy St., Newark, DE 19716, USA. E-mail: vlachos@udel.edu*
[b] *Delaware Energy Institute, University of Delaware, 221 Academy St., Newark, DE 19716, USA*
[c] *Center for Plastics Innovation, University of Delaware, 221 Academy St., Newark, DE 19716, USA*

† Electronic supplementary information (ESI) available. See DOI: https://doi.org/10.1039/d4cy01118j

amorphous silica supports, the challenge is compounded by the absence of structural uniformity.[19,20] Characterization methods, such as EXAFS and XANES, provide space-averaged information rather than the local structural features of the grafted site that catalyze the reaction. Not all spectroscopically relevant sites, or the most abundant sites, are necessarily catalytically active. For instance, in the Phillips catalyst ($Cr@SiO_2$), only 10% of the sites are active.[21] $Co@SiO_2$ presents a similar case, where small but detectable amounts of Co(III) are present in the as-synthesized $Co@SiO_2$ catalyst.[22] This necessitates consideration of other possible sites to explore possible local geometries in mechanistic investigations that may or may not have been picked up in experiments. To make progress, we first need to eliminate ambiguities related to the reaction mechanisms and how they are influenced by the structural properties of the active site.

In this contribution, we focus on ethane-to-ethylene dehydrogenation on various structural models of the active site of silica-supported mononuclear Fe(II) and Fe(III). With the aid of electronic structure calculations, we elucidate open questions related to the dehydrogenation mechanism. We consider tricoordinate and tetracoordinate Fe(II) sites and determine that σ-metathesis is an unlikely dehydrogenation mechanism on $Fe(II)@SiO_2$, regardless of the coordination geometry. On $Fe(II)@SiO_2$, the kinetically favored pathway involves heterolytic C–H activation by a siloxide pair Fe–OSi–, followed by β-hydride elimination facilitated by spin-crossing, akin to $Co(II)@SiO_2$. However, the energetics and dynamics of the spin crossover phenomena during the rate-limiting β-H elimination of supported Fe(II) and Co(II) are different, in contrast to the corresponding alkyl complexes in organometallic chemistry.[23,24] We show that $Fe(III)@SiO_2$ exhibits a more complex behavior and present a new redox dehydrogenation mechanism which, energetically, is on a par with the heterolytic mechanism on $Co(II)/SiO_2$.

2. Methods

Electronic structure calculations were performed in Gaussian 09 version d01 (ref. 25) using the long-range-corrected hybrid functional CAM-B3LYP[26] and the triple-ζ (def2TZVP) basis set for all atoms. CAM-B3LYP has been benchmarked for systems exhibiting charge transfer and against experimental spin-crossover enthalpies of organometallic Fe(II) and Fe(III) complexes.[27] We performed vibrational frequency analysis to confirm the character of all stationary points. To corroborate the correct link between the transition states and corresponding minima, we performed intrinsic reaction coordinate (IRC) calculations. Thermal corrections to the electronic energies were computed at 898.15 K. We followed the protocol established by Srinivas *et al.*[10] to compute the tunneling factor at the minimum energy crossing point (MECP). We used the formalism of Harvey[28] to obtain an estimate of the MECP, followed by vibration frequency analysis using GLOWfreqs[29] to confirm the nature of MECP. Spin–orbit coupling constants were estimated using the methodology by Bellows *et al.*[23]

3. Results and discussion

First, we discuss catalytic pathways on structural models of the Fe(II) active site. We considered the siloxane cluster[30] shown in Fig. 1a and created tetrahedrally coordinated Fe(II) sites by deprotonating two silanol (–SiOH) groups. Tetrahedral Fe(II) silicates are reported in organometallics[31,32] and in oxides such as Fe_2SiO_4 (ref. 33 and 34) and synthetic glasses.[35] With a formal charge of −2 on the cluster model, the formal charge on the Fe atom was +2 (d^6 configuration), making the system electroneutral. In the model shown in Fig. 1a, the tetrahedral Fe atom is coordinated by two silanolate groups ($–SiO^-$), one siloxane (–Si–O–Si–) oxygen and one silanol group. The 3-coordinate Fe(II) active site model (Fig. 1b) was hewn out of the 4-coordinate model and the Fe(II) center was coordinated to two $–SiO^-$ ligands and one –Si–O–Si– group. All dangling bonds in the siloxane clusters were capped with H atoms which were held fixed throughout the subsequent geometry optimization and transition state calculations. Fluorine and hydroxyl (OH) have been investigated as alternate capping agents on the siloxane cluster model for the Cr/SiO_2 catalyst to study ethylene polymerization reaction, and were shown to have minimal effect on the activation barriers.[36] In general, –OH group introduces spurious hydrogen bonds and is thus avoided.[19] Our choice of H atom termination is in line with prior works.[37,38] We further cleaved the tetrahedral cluster to generate the tricoordinate Fe(II) structure, in accordance with the EXAFS results of Hu *et al.*[5] shown in Fig. 1b. Although Guo *et al.*[39] have identified and Toraman *et al.*[40] have confirmed carburized Fe species, we did not model such active sites as they become relevant only at temperatures much higher than those for dehydrogenation. Small cluster models have been previously used to investigate atomically dispersed 3d metals on the silica surface such as Cr/SiO_2,[41–43] V/SiO_2,[44] Co/SiO_2 (ref. 8 and 10) and Zn/SiO_2 (ref. 9) with the implicit assumption that the electronic effects are localized, making small cluster models reasonably accurate. Minimal cluster models are typically preferred as they make no structural assumptions about the support,[19] with a growing body of evidence that larger models show comparable results as the smaller ones.[45] The ground

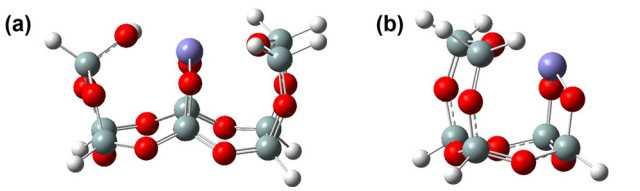

Fig. 1 Structural models of the $Fe(II)@SiO_2$ active sites. (a) 4-Coordinate geometry. (b) 3-Coordinate geometry (purple: Fe; red: O; white: H; teal: Si.).

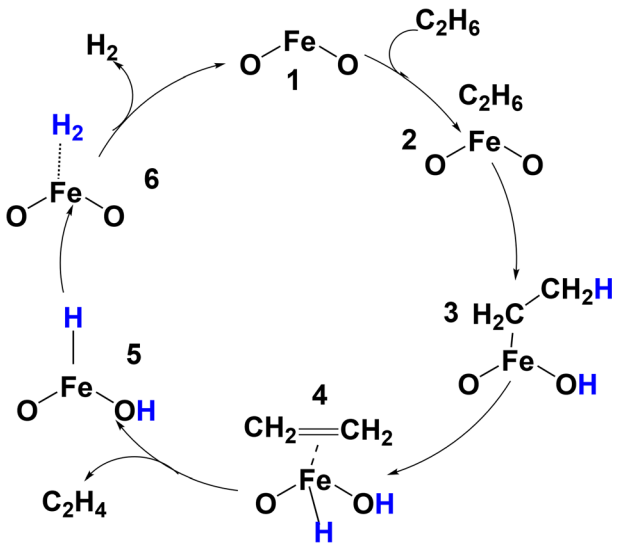

Fig. 2 Ethane dehydrogenation on Fe(II)@SiO_2. Heterolytic C–H activation and β-H elimination.

electronic state of the Fe d^6 bare active site is the quintet, as expected in the weak-field ligand environment of silica. Hereafter, the spin state of an intermediate or transition state will be indicated by a superscript, and the coordination geometry of Fe is indicated by a subscript, "t" for 3-coordinate and "tet" for 4-coordinate.

On both the tricoordinate and tetracoordinate Fe d^6 structural models, we tested the dehydrogenation mechanism shown in Fig. 2. The corresponding potential energy profiles and transition states are shown in Fig. 3(a) and (b), respectively. Following the ethane coordination to Fe (**2**), the C–H bond is activated by the metal center and a $–SiO^-$ ligand that abstracts the hydrogen, forming the metal ethyl intermediate **3** and a –SiOH. The ground electronic state remains a quintet, regardless of the Fe's coordination geometry. However, the 3-coordinate site presents a slightly lower intrinsic C–H activation barrier than the 4-coordinate model by about 0.14 eV (1.68 eV on the 3-coordinate *vs.* 1.82 eV on the 4-coordinate). The C–H activation is indeed heterolytic as analysis of the Mulliken spin densities ruled out a proton-coupled electron transfer (PCET) mechanism (ESI† Table S1). In a PCET mechanism, the abstracted hydrogen atom would still have ended up on the oxygen atom as a proton, but its electron would have been transferred to the metal center. The Mulliken analysis showed 4 unpaired electrons on Fe d^6, indicating no reduction, and zero spin density on the abstracted H and on the carbon atom of **3**. The spins on the oxygen ligands remained quenched. The Fe–C bond distance in ^{5}**3** is 2.0 Å in the 3-coordinate site and 2.06 Å in the 4-coordinate, both in good agreement with the distance of 1.96 Å reported in Hu *et al.*'s[5] EXAFS studies of the as-prepared and H_2 pretreated Fe(II)@SiO_2 catalyst at 400 °C.

TS_{ag} in Fig. 3 refers to the agostic transition state in the tetra-coordinate site preceding the β-hydride elimination step, and it involves the H2 atom (atom labelling in Fig. 4) coordinated to both the C_2H_5 moiety and the Fe (see Fig. S1 in the ESI†). Unlike the tetracoordinate site, which is sterically hindered, the tricoordinate site did not present any agostic transition state and intermediate **3** in Fig. 3(a) is already an agostic product. We arrive at this conclusion due to geometric similarities between intermediates $\mathbf{3_{ag}}$ and **3** and evidence from literature.[23] However, the agostic intermediate is mechanistically inconsequential as it precedes the spin-crossing event.

As can be seen from the electronic energy profiles in Fig. 3 during the ensuing β-H elimination from the Fe-ethyl intermediate (^{5}**3**), the Fe d^6 atom undergoes a spin flip into the triplet state, which lies lower in energy than the quintet. Spin pairing is induced by spin–orbit coupling and empties a metal d-orbital to accommodate the formation of the metal-

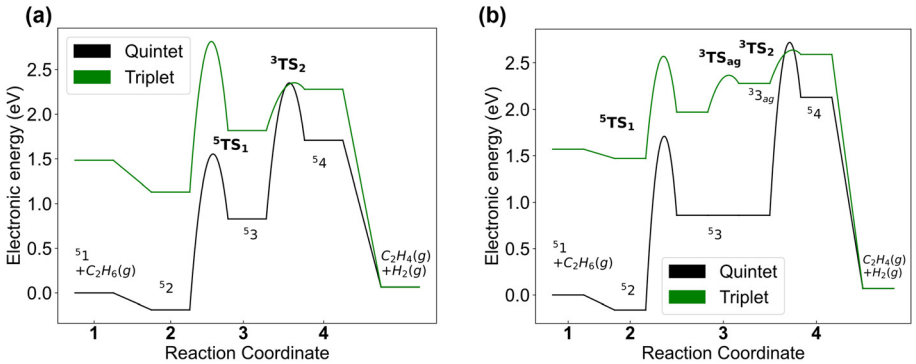

Fig. 3 Electronic energy profiles for the mechanism shown in Fig. 2 on Fe(II)@SiO_2 sites. (a) 3-Coordinate Fe(II) geometry. (b) 4-Coordinate Fe(II) geometry. The profiles correspond to the two lowest-lying spin states, the quintet and the triplet. Relevant intermediates and transition states (in bold) are indicated in the energy profile with spin states in superscripts. Quintet to triplet spin-crossing takes place prior to the β-H elimination transition state. In (b), note the agostic intermediate (and associated transition state $^3TS_{ag}$) preceding the β-H elimination transition state ($^3TS_2$) in the triplet spin state. Intermediate **1** is the reference state, with energy equal to the sum of energies of the bare active site and C_2H_6(g). Intermediates **2**–**4** are surface bound species. C_2H_4(g) + H_2(g) are the gaseous products of the reaction pathway, and the energy level is obtained by subtracting the DFT energy of C_2H_4(g) + H_2(g) from C_2H_6(g). Full mechanism including the hydrogen recombination step is presented in Fig. S2† of the accompanying ESI.†

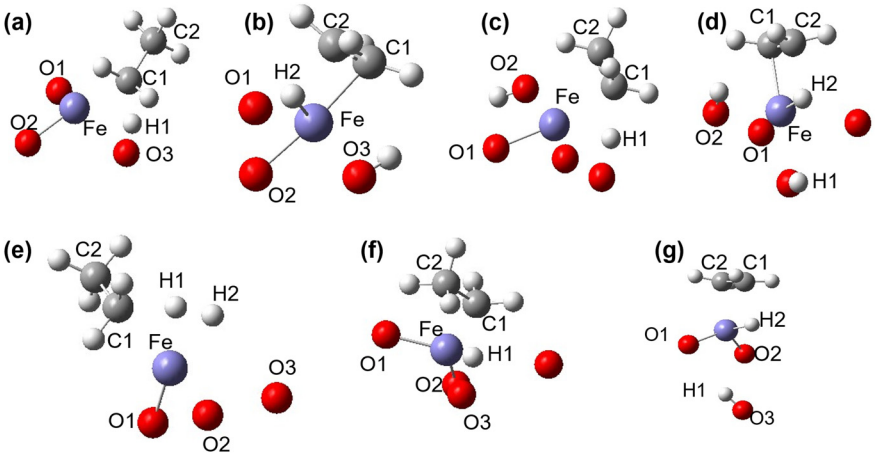

Fig. 4 Transition state geometries obtained in this work. Heterolytic cleavage mechanism: (a) $^5TS_1$, (b) $^3TS_2$ on the tricoordinate site; (c) $^5TS_1$, (d) $^3TS_2$ on the tetracoordinate site; (e) $^5TS_3$ of the metathesis mechanism on the tricoordinate site; redox mechanism: (f) $^6TS_1$ and (g) $^4TS_2$ on the tetracoordinate site. Superscript denotes the spin state, and subscript denotes the reaction number in the corresponding reaction mechanism (heterolytic cleavage: Fig. 2, σ-bond metathesis: Fig. 5 and redox: Fig. 6(b)). Only the active site is shown for clarity (purple: Fe; red: O; white: H; grey: C.).

hydride. It is typical in high-spin complexes and has been reported for the $Fe(C_2H_5)^+$ cation,[46] diketiminate-supported $Fe(C_2H_5)$ complexes[23] and several other systems.[47] Because of the spin-crossing, the repulsive three-electron two-orbital interaction in the high-spin state becomes an attractive two-electron two-orbital interaction in the low-spin state, which lowers the β-H elimination barrier (see Fig. 5). Regardless of the coordination geometry of the active site Fe (3-coordinate or 4-coordinate), the triplet transition state assumes square planar geometry, typical of low-spin complexes. As can been seen from Fig. 2, past the β-H elimination transition state, the complex crosses over back to the quintet state, which is the ground electronic state of the metal-hydride (see Fig. 4b and d for β-H elimination transition state on tricoordinate and tetracoordinate site, respectively). Similar spin-crossing events have been reported by Srinivas *et al.*[10] for atomically dispersed Co d^7 on silica. Unlike Co, however, spin–orbit coupling in Fe is not strong and this has a couple of implications. First, the low-spin β-H elimination transition state is not significantly lower than the high-spin one compared to the corresponding states in Co(II)@SiO_2, explaining the lower activity for small alkane dehydrogenation observed in experiments.[5] It must be noted, however, that the quintet-triplet gap is noticeably smaller for the 3-coordinate than the 4-coordinate geometry, presumably because the former affords the system greater flexibility. Second, the dynamics of the β-H elimination is non-adiabatic with a tunneling constant of 0.86, lower than that obtained for Co(II)@SiO_2 corresponding to an adiabatic transition.[10]

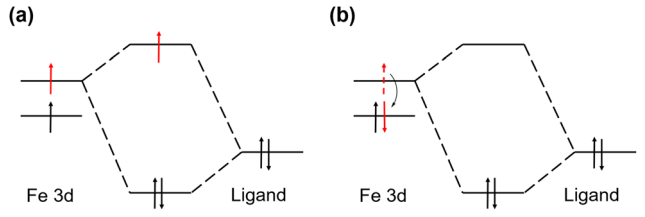

Fig. 5 Molecular orbital diagram showing the interaction corresponding to β-hydride elimination on (a) quintet (high spin) and (b) triplet (low spin) Fe(II)@SiO_2. Similar interactions can also be applied to the spin states in Fe(III)@SiO_2.

At high temperatures, entropic contributions are dominant.[48] The entropies of formation of the transition state is negative for both C–H activation steps, in alignment with the dissociative nature of these steps. Free energy barriers are higher than electronic energies (see Fig. S3 in the ESI†). The rate determining step is the β hydride elimination step in the heterolytic cleavage mechanism, the same as that for Co(II)@SiO_2. High-spin states result in longer bond lengths due to repulsion within the occupied orbitals, making the transition states more flexible and contributing more to the entropic term. In contrast, low-spin states have tightly bound transition states with shorter bonds, leading to lesser entropic corrections. This leads to the flipping of the spin state order at reaction temperatures in the free energy diagrams, further suggesting the minimal benefit from spin crossover during β-hydride elimination. The hydrogen recombination step has a lower free energy change because the elementary step is an association reaction with partial H-H bond formation.

Instead of the hydrogen recombination (**6**) completing the cycle, as shown in Fig. 2, it has been proposed[5] that the metal-hydride **5** could react with incoming ethane as shown in Fig. 6 (intermediate **7**). Through a σ-metathesis mechanism, the metal-ethyl intermediate could then form with concomitant release of H_2. This is the general metathesis mechanism for a d^6 center and involves discrete σ-complexes undergoing ligand exchange.[49] Once the metal-ethyl intermediate has formed, β-H elimination could ensue, as described earlier. We tested this hypothesis[12] and were

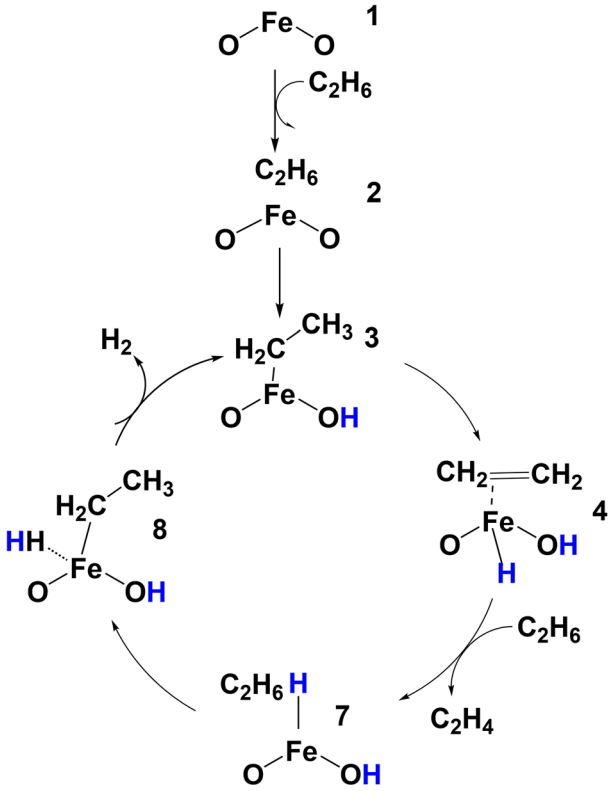

Fig. 6 Ethane dehydrogenation on Fe(II)@SiO_2. σ-Bond metathesis mechanism.

able to optimize the related intermediates and transition states (see Fig. 4e) for the 3-coordinate active site. We were unable, however, to identify the respective intermediates and transition states for the 4-coordinate site, possibly because this geometry does not afford the active site complex sufficient flexibility to accommodate six ligands on the metal center. For the 3-coordinate geometry, the σ-bond metathesis requires significant activation energy, with an overall energy span near 3.5 eV (Fig. S4,† TS_3), making this pathway very unlikely compared with the mechanism in Fig. 2. The ligand exchange step presents a high free energy barrier as shown in Fig. S5 of the ESI.†

A redox mechanism has been proposed by Lobo and co-workers[17] for the dehydrogenation of propane to propylene on isomorphously substituted H–[Fe(III)]-ZSM5 adapted for ethane the mechanism is depicted in Fig. 7a. In that mechanism, the Fe d^5 atom is first reduced by accepting an electron from the bound ethane molecule. Next, the unstable ethane radical ($C_2H_6^{\bullet+}$) releases H_2 and the resulting $C_2H_4^{\bullet+}$ radical accepts the electron back from Fe, which returns to the 3+ oxidation state. Although never computationally confirmed to the best of our knowledge, it raises the intriguing possibility of a redox mechanism of C–H activation on atomically dispersed Fe(III) on amorphous SiO_2. A C–H bond may in principle be activated by metal-oxygen pairs on transition metal oxides, either through a hydrogen atom transfer (HAT) mechanism or through a PCET mechanism.[50,51] In the HAT mechanism, the reaction essentially proceeds through the formation of radicals: an H atom is abstracted by the oxygen of the metal-oxide pair while the alkyl radical coordinates to the metal center. In the PCET mechanism, as described above, the abstracted hydrogen atom ends up on the oxygen atom as a proton while its electron is transferred to the metal center, which is reduced as a result.

We tested the possibility of a redox dehydrogenation mechanism on an Fe(III)@SiO_2 site. We used the structural model shown in Fig. 8. In this, the Fe atom was grafted on three SiO^- groups, making it formally d^5. We considered different spin states for the bare active site and the one with multiplicity 6 was the ground electronic state. Remarkably, analysis of the Mulliken spin density of the bare active site showed that the Fe center had 4 unpaired α-electrons instead of 5, which means that Fe was autoreduced to the d^6 state. The spin density values

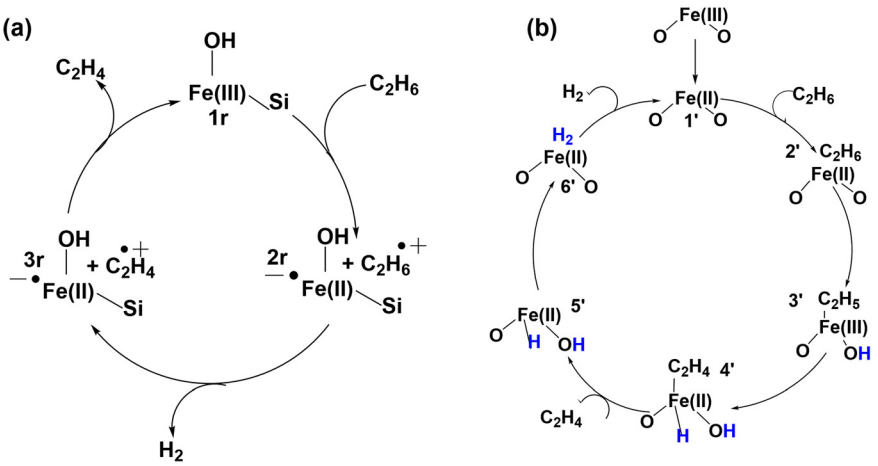

Fig. 7 Dehydrogenation mechanism on Fe(III)@SiO_2. (a) Redox mechanism proposed by Yun and Lobo (ref. 16). (b) Revised redox mechanism proposed in this work. In (b), Fe(III) is unstable and spontaneously undergoes reduction to the Fe(II) state while the system.

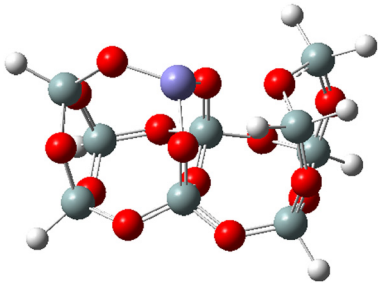

Fig. 8 Structural model of the Fe(III)@SiO_2 active site. The Fe center is coordinated to 3 silanolate ligands (purple: Fe; red: O; white: H; teal: Si.).

Table 1 Mulliken spin densities related to the redox mechanism presented in Fig. 6(b) (atom labelling scheme in Fig. 4)

Species	Fe	O1	O2	O3	C1	H1/H2
^{6}1′	4.18	0.25	0.26	0.24	0	0
^{6}TS	4.20	0.24	0.104	0.18	0.16	0.02
^{4}3′	3.37	0.08	0.09	0	−0.55	0.014
^{4}TS	3.17	0.13	0	0.13	−0.22	−0.32 (H2)
^{6}4′	4.25	0.2	0	0.21	0.08	−0.22 (H2)

are listed in Table 1 and spin density plots are shown in Fig. S6.†

The spin densities on the oxygen atoms of the ligands showed that the β-electron that transferred to the Fe atom originated from one of the SiO^- ligands. In addition, the majority spin density on the silanolate ligands was delocalized over the oxygen atoms of all three of them, conserving the total spin multiplicity of 6. Thus, it appears that Fe d^5 is not stable in the environment of three silanolate ligands on amorphous silica. The immediate implication, therefore, is that the dehydrogenation of ethane to ethylene would not proceed via the redox mechanism in Fig. 7a. That notwithstanding, we proceeded to investigate the full dehydrogenation mechanism, curious to explore the mechanistic implications of the delocalized spin density on the SiO^- ligands and whether the mechanism would be similar to the one we presented in Fig. 2 for the Fe d^6 site with two SiO^- ligands. Our calculations showed that the system retained the multiplicity of 6 both upon ethane binding and at the C–H activation transition state (see Fig. 4f). However, we found spin-crossing over to the more stable quartet state upon formation of the Fe-alkyl intermediate; the H atom was accepted by a SiO^- ligand with Fe coordinated to the three surface oxygens and the carbon atom of the alkyl group (this is in stark contrast with the mechanism over Fe(II)@SiO_2, shown in Fig. 2, where spin-crossing from the quintet to the triplet occurred after the Fe-alkyl intermediate had formed and before the β-H elimination.). In the quartet state of the Fe-alkyl intermediate, the spin density of the Fe atom indicated about 3 unpaired electrons—it was 4 prior to the spin-crossing. In addition, in the quartet state, the spin density on the SiO^- oxygen atoms were fully quenched, and the transferred H atom carried no spin density. Taken together, the calculations showed that the C–H bond broke heterolytically in the sextet state and, upon formation of the Fe-alkyl intermediate, the Fe atom was re-oxidized from the d^6 to the d^5 electronic configuration by donating an electron back to oxygen ligands, quenching their spins. As a result, the Fe atom ended up with an empty d-orbital which prepared the system for the β-H elimination over the quartet transition state (Fig. 4g), as can been seen in Fig. 9. The system returned to the sextet spin state upon formation of the metal-hydride intermediate and ethylene. Based on this analysis, in Fig. 7b, we present the revised redox mechanism.

The energy requirements are quite favorable compared with the mechanism on Fe(II)@SiO_2. The highest-lying transition state in the redox mechanism is at *ca.* 1.6 eV and it corresponds to the C–H activation. In the heterolytic mechanism on 3-coordinate Fe(II)@SiO_2, the highest-lying transition state is at *ca.* 2.3 eV and it is associated with the β-H elimination. The 1.6 eV barrier also compares favorably with the 1.5 eV barrier (β-H elimination) calculated by Srinivas *et al.*[10] on Co(II)@SiO_2. The rate-determining step in the redox pathway on Fe(III)@SiO_2 is the first C–H activation step with a significantly lower energy barrier compared to the heterolytic cleavage pathway, as shown in Fig. S8 of the ESI.† In the redox mechanism, the spin state ordering is conserved in the free energy profile unlike the heterolytic pathway.

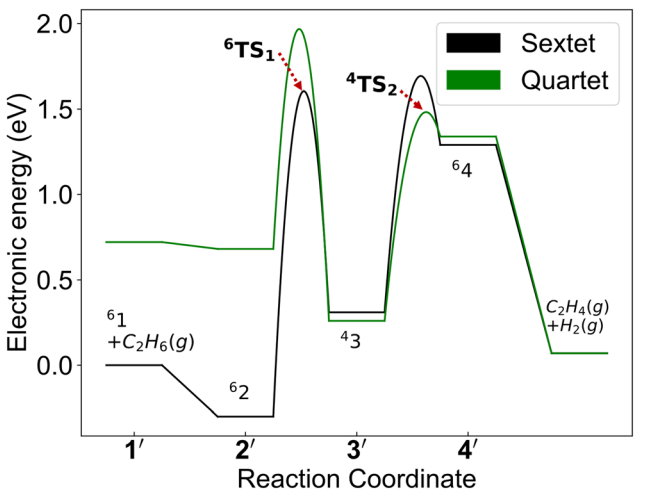

Fig. 9 Electronic energy profiles for the redox mechanism shown in Fig. 7(b) on initially prepared Fe(III)@am–SiO_2. The profiles correspond to the two lowest-lying spin states with spin multiplicities 6 and 4. Relevant intermediates and transition states (in bold) are indicated in the energy profile with spin states in superscripts. Intermediate **1** is the reference state, with energy equal to the sum of energies of the bare active site and C_2H_6(g). Intermediates **2**–**4** are surface bound species. C_2H_4(g) + H_2(g) are gas phase ethylene and hydrogen gas generated as part of the catalytic cycle. Full mechanism including the hydrogen recombination step is presented in Fig. S7 of the accompanying ESI.† The overall reaction is endothermic. Complete free energy profile is shown in Fig. S8 of the ESI.†

4. Conclusions

We have elucidated open questions related to the catalytic behavior of silica-supported mononuclear Fe(II) and Fe(III) catalysts for ethane dehydrogenation. We determined that σ-metathesis is an unlikely dehydrogenation mechanism. On Fe(II)@SiO_2, irrespective of coordination, the reaction proceeds with heterolytic C–H bond activation by a siloxide (Fe–OSi–) pair, followed by β-hydride elimination facilitated by spin-crossing. Isolated Fe(III) grafted on SiO_2 exhibits a more nuanced behavior. In the high-spin sextet state, Fe(III) spontaneously undergoes autoreduction to the 2+ state by a silanolate ligand. The metal center is re-oxidized to the +3 state as a result of spin-crossing to the low-spin quartet state upon formation of the Fe-ethyl intermediate, which forms by heterolytic activation of the C–H bond. In the 3+ quartet state, Fe has an empty d-orbital which facilitates the β-elimination, upon completion of which Fe returns to the 2+ oxidation. This redox mechanism is energetically on a par with the heterolytic mechanism on Co(II)/SiO_2. We hope that these findings will spur further experimentation in iron chemistry for C–H activation.

Data availability

The data supporting this article has been included as part of the ESI.†

Author contributions

Sakshi S. performed the calculations and data analysis and wrote the manuscript. Sanjana S. provided guidance at the initial stages of the project and contributed to the manuscript. D. G. V. designed the project. S. C. supervised the project and performed data analysis. All authors edited the manuscript.

Conflicts of interest

The authors declare no competing interests.

Acknowledgements

The authors gratefully acknowledge the support from the Department of Energy, Office of Fossil Energy (DE-FE0031877). The authors are deeply grateful to the contributions of Dr. Stavros Caratzoulas, who sadly passed away during the preparation of this work.

References

1 J. Balleli, The Shale Gas "revolution" in the United States: Global Implications, Options for the EU, *Policy Briefing*, Belgium, 2013, pp. 491–498, **https://www.europarl.europa.eu/RegData/etudes/briefing_note/join/2013/491498/EXPO-AFET_SP%282013%29491498_EN.pdf**.

2 E. McFarland, Unconventional Chemistry for Unconventional Natural Gas, *Science*, 2012, **338**(6105), 340–342, DOI: **10.1126/science.1226840**.

3 R. M. Bullock, J. G. Chen, L. Gagliardi, P. J. Chirik, O. K. Farha, C. H. Hendon, C. W. Jones, J. A. Keith, J. Klosin, S. D. Minteer, R. H. Morris, A. T. Radosevich, T. B. Rauchfuss, N. A. Strotman, A. Vojvodic, T. R. Ward, J. Y. Yang and Y. Surendranath, Using Nature's Blueprint to Expand Catalysis with Earth-Abundant Metals, *Science*, 2020, **369**(6505), eabc3183, DOI: **10.1126/science.abc3183**.

4 S. Mitchell and J. Pérez-Ramírez, Single Atom Catalysis: A Decade of Stunning Progress and the Promise for a Bright Future, *Nat. Commun.*, 2020, **11**(1), 4302, DOI: **10.1038/s41467-020-18182-5**.

5 B. Hu, N. M. Schweitzer, G. Zhang, S. J. Kraft, D. J. Childers, M. P. Lanci, J. T. Miller and A. S. Hock, Isolated Fe ^{II} on Silica As a Selective Propane Dehydrogenation Catalyst, *ACS Catal.*, 2015, **5**(6), 3494–3503, DOI: **10.1021/acscatal.5b00248**.

6 D. P. Estes, G. Siddiqi, F. Allouche, K. V. Kovtunov, O. V. Safonova, A. L. Trigub, I. V. Koptyug and C. Copéret, C–H Activation on Co,O Sites: Isolated Surface Sites versus Molecular Analogs, *J. Am. Chem. Soc.*, 2016, **138**(45), 14987–14997, DOI: **10.1021/jacs.6b08705**.

7 K. Yu, S. Srinivas, C. Wang, W. Chen, L. Ma, S. N. Ehrlich, N. Marinkovic, P. Kumar, E. A. Stach, S. Caratzoulas, W. Zheng and D. G. Vlachos, High-Temperature Pretreatment Effect on Co/SiO $_2$ Active Sites and Ethane Dehydrogenation, *ACS Catal.*, 2022, **12**(19), 11749–11760, DOI: **10.1021/acscatal.2c03180**.

8 B. Hu, A. Getsoian, N. M. Schweitzer, U. Das, H. Kim, J. Niklas, O. Poluektov, L. A. Curtiss, P. C. Stair, J. T. Miller and A. S. Hock, Selective Propane Dehydrogenation with Single-Site CoII on SiO2 by a Non-Redox Mechanism, *J. Catal.*, 2015, **322**, 24–37, DOI: **10.1016/j.jcat.2014.10.018**.

9 N. M. Schweitzer, B. Hu, U. Das, H. Kim, J. Greeley, L. A. Curtiss, P. C. Stair, J. T. Miller and A. S. Hock, Propylene Hydrogenation and Propane Dehydrogenation by a Single-Site Zn $^{2+}$ on Silica Catalyst, *ACS Catal.*, 2014, **4**(4), 1091–1098, DOI: **10.1021a/cs401116p**.

10 S. Srinivas, D. G. Vlachos and S. Caratzoulas, Spin-Crossing in Heterogeneous Ethane Dehydrogenation by Atomically Dispersed Co/SiO2, *Chem Catal.*, 2023, **3**(4), 100534, DOI: **10.1016/j.checat.2023.100534**.

11 P. Wang, H. Wu, X.-P. Zhang, G. Huang, R. H. Crabtree and X. Li, Sigma-Bond Metathesis as an Unusual Asymmetric Induction Step in Rhodium-Catalyzed Enantiodivergent Synthesis of C–N Axially Chiral Biaryls, *J. Am. Chem. Soc.*, 2023, jacs.3c00003, DOI: **10.1021/jacs.3c00003**.

12 R. N. Perutz and S. Sabo-Etienne, The σ-CAM Mechanism: σ Complexes as the Basis of σ-Bond Metathesis at Late-Transition-Metal Centers, *Angew. Chem., Int. Ed.*, 2007, **46**(15), 2578–2592, DOI: **10.1002/anie.200603224**.

13 C. Nozaki, C. G. Lugmair, A. T. Bell and T. D. Tilley, Synthesis, Characterization, and Catalytic Performance of Single-Site Iron(III) Centers on the Surface of SBA-15 Silica, *J. Am. Chem. Soc.*, 2002, **124**(44), 13194–13203, DOI: **10.1021/ja020388t**.

14 M. Cheng, H. Zhao, J. Yang, J. Zhao, L. Yan, H. Song and L. Chou, The Catalytic Dehydrogenation of Isobutane and the Stability Enhancement over Fe Incorporated SBA-15,

Microporous Mesoporous Mater., 2018, **266**, 117–125, DOI: **10.1016/j.micromeso.2018.02.046**.

15 N. A. Grosso-Giordano, A. J. Yeh, A. Okrut, D. J. Xiao, F. Grandjean, G. J. Long, S. I. Zones and A. Katz, Effect of Defect Site Preorganization on Fe(III) Grafting and Stability: A Comparative Study of Delaminated Zeolite vs Amorphous Silica Supports, *Chem. Mater.*, 2017, **29**(15), 6480–6492, DOI: **10.1021/acs.chemmater.7b02062**.

16 J. H. Yun and R. F. Lobo, Catalytic Dehydrogenation of Propane over Iron-Silicate Zeolites, *J. Catal.*, 2014, **312**, 263–270, DOI: **10.1016/j.jcat.2014.02.007**.

17 J. H. Yun and R. F. Lobo, Radical Cation Intermediates in Propane Dehydrogenation and Propene Hydrogenation over H-[Fe] Zeolites, *J. Phys. Chem. C*, 2014, **118**(47), 27292–27300, DOI: **10.1021/jp504453n**.

18 D. Balcells, E. Clot and O. Eisenstein, C—H Bond Activation in Transition Metal Species from a Computational Perspective, *Chem. Rev.*, 2010, **110**(2), 749–823, DOI: **10.1021/cr900315k**.

19 B. R. Goldsmith, B. Peters, J. K. Johnson, B. C. Gates and S. L. Scott, Beyond Ordered Materials: Understanding Catalytic Sites on Amorphous Solids, *ACS Catal.*, 2017, **7**(11), 7543–7557, DOI: **10.1021/acscatal.7b01767**.

20 M. F. Delley, G. Lapadula, F. Núñez-Zarur, A. Comas-Vives, V. Kalendra, G. Jeschke, D. Baabe, M. D. Walter, A. J. Rossini, A. Lesage, L. Emsley, O. Maury and C. Copéret, Local Structures and Heterogeneity of Silica-Supported M(III) Sites Evidenced by EPR, IR, NMR, and Luminescence Spectroscopies, *J. Am. Chem. Soc.*, 2017, **139**(26), 8855–8867, DOI: **10.1021/jacs.7b02179**.

21 C. Copéret, A. Comas-Vives, M. P. Conley, D. P. Estes, A. Fedorov, V. Mougel, H. Nagae, F. Núñez-Zarur and P. A. Zhizhko, Surface Organometallic and Coordination Chemistry toward Single-Site Heterogeneous Catalysts: Strategies, Methods, Structures, and Activities, *Chem. Rev.*, 2016, **116**(2), 323–421, DOI: **10.1021/acs.chemrev.5b00373**.

22 G. Grzybek, M. Greluk, P. Patulski, P. Stelmachowski, K. Tarach, G. Słowik, M. Rotko, S. Valencia, F. Rey and K. Góra-Marek, Adjustment of the ZSM-5 Zeolite Support towards the Efficient Hydrogen Production by Ethanol Steam Reforming on Cobalt Catalysts, *Chem. Eng. J.*, 2023, **467**, 143239, DOI: **10.1016/j.cej.2023.143239**.

23 S. M. Bellows, T. R. Cundari and P. L. Holland, Spin Crossover during β-Hydride Elimination in High-Spin Iron(II)– and Cobalt(II)–Alkyl Complexes, *Organometallics*, 2013, **32**(17), 4741–4751, DOI: **10.1021/om400325x**.

24 T. Takayanagi, K. Saito, H. Suzuki, Y. Watabe and T. Fujihara, Computational Analysis of Two-State Reactivity in β-Hydride Elimination Mechanisms of Fe(II)– and Co(II)–Alkyl Complexes Supported by β-Diketiminate Ligand, *Organometallics*, 2019, **38**(19), 3582–3589, DOI: **10.1021/acs.organomet.9b00418**.

25 M. J. Frisch, *Gaussian*, 2016.

26 T. Yanai, D. P. Tew and N. C. Handy, A New Hybrid Exchange–Correlation Functional Using the Coulomb-Attenuating Method (CAM-B3LYP), *Chem. Phys. Lett.*, 2004, **393**(1–3), 51–57, DOI: **10.1016/j.cplett.2004.06.011**.

27 O. S. Siig and K. P. Kepp, Iron(II) and Iron(III) Spin Crossover: Toward an Optimal Density Functional, *J. Phys. Chem. A*, 2018, **122**(16), 4208–4217, DOI: **10.1021/acs.jpca.8b02027**.

28 J. N. Harvey, M. Aschi, H. Schwarz and W. Koch, The Singlet and Triplet States of Phenyl Cation. A Hybrid Approach for Locating Minimum Energy Crossing Points between Non-Interacting Potential Energy Surfaces, *Theor. Chem. Acc.*, 1998, **99**(2), 95–99, DOI: **10.1007/s002140050309**.

29 K. L. Gannon, M. A. Blitz, C.-H. Liang, M. J. Pilling, P. W. Seakins, D. R. Glowacki and J. N. Harvey, An Experimental and Theoretical Investigation of the Competition between Chemical Reaction and Relaxation for the Reactions of 1CH2 with Acetylene and Ethene: Implications for the Chemistry of the Giant Planets, *Faraday Discuss.*, 2010, **147**, 173, DOI: **10.1039/c004131a**.

30 M. F. Delley, F. Núñez-Zarur, M. P. Conley, A. Comas-Vives, G. Siddiqi, S. Norsic, V. Monteil, O. V. Safonova and C. Copéret, Proton Transfers Are Key Elementary Steps in Ethylene Polymerization on Isolated Chromium(III) Silicates, *Proc. Natl. Acad. Sci. U. S. A.*, 2014, **111**(32), 11624–11629, DOI: **10.1073/pnas.1405314111**.

31 S. C. Bart, E. J. Hawrelak, A. K. Schmisseur, E. Lobkovsky and P. J. Chirik, Synthesis, Reactivity, and Solid State Structures of Four-Coordinate Iron(II) and Manganese(II) Alkyl Complexes, *Organometallics*, 2004, **23**(2), 237–246, DOI: **10.1021/om034188h**.

32 F. Cotton and G. Wilkinson, *Advanced Inorganic Chemistry*, New York Wiley, 1980.

33 W. E. Jackson, J. M. De Leon, G. E. Brown, G. A. Waychunas, S. D. Conradson and J.-M. Combes, High-Temperature XAS Study of Fe $_2$ SiO $_4$ Liquid: Reduced Coordination of Ferrous Iron, *Science*, 1993, **262**(5131), 229–233, DOI: **10.1126/science.262.5131.229**.

34 T. F. Cooney and S. K. Sharma, Structure of Glasses in the Systems Mg2SiO4·Fe2SiO4, Mn2SiO4·Fe2SiO4, Mg2SiO4·CaMgSiO4, and Mn2SiO4·CaMnSiO4, *J. Non-Cryst. Solids*, 1990, **122**(1), 10–32, DOI: **10.1016/0022-3093(90)90220-G**.

35 G. A. Waychunas, G. E. Brown, C. W. Ponader and W. E. Jackson, Evidence from X-Ray Absorption for Network-Forming Fe2+ in Molten Alkali Silicates, *Nature*, 1988, **332**(6161), 251–253, DOI: **10.1038/332251a0**.

36 A. Fong, Y. Yuan, S. L. Ivry, S. L. Scott and B. Peters, Computational Kinetic Discrimination of Ethylene Polymerization Mechanisms for the Phillips (Cr/SiO $_2$) Catalyst, *ACS Catal.*, 2015, **5**(6), 3360–3374, DOI: **10.1021/acscatal.5b00016**.

37 J. Sauer, Molecular Models in Ab Initio Studies of Solids and Surfaces: From Ionic Crystals and Semiconductors to Catalysts, *Chem. Rev.*, 1989, **89**(1), 199–255, DOI: **10.1021/cr00091a006**.

38 N. Lopez, G. Pacchioni, F. Maseras and F. Illas, Hybrid Quantum-Mechanical and Molecular Mechanics Study of Cu

Atoms Deposition on SiO2 Surface Defects, *Chem. Phys. Lett.*, 1998, **294**(6), 611–618, DOI: **10.1016/S0009-2614(98)00907-5**.

39 X. Guo, G. Fang, G. Li, H. Ma, H. Fan, L. Yu, C. Ma, X. Wu, D. Deng, M. Wei, D. Tan, R. Si, S. Zhang, J. Li, L. Sun, Z. Tang, X. Pan and X. Bao, Direct, Nonoxidative Conversion of Methane to Ethylene, Aromatics, and Hydrogen, *Science*, 2014, **344**(6184), 616–619, DOI: **10.1126/science.1253150**.

40 H. E. Toraman, K. Alexopoulos, S. C. Oh, S. Cheng, D. Liu and D. G. Vlachos, Ethylene Production by Direct Conversion of Methane over Isolated Single Active Centers, *Chem. Eng. J.*, 2021, **420**, 130493, DOI: **10.1016/j.cej.2021.130493**.

41 A. Fong, B. Peters and S. L. Scott, One-Electron-Redox Activation of the Reduced Phillips Polymerization Catalyst, via Alkylchromium(IV) Homolysis: A Computational Assessment, *ACS Catal.*, 2016, **6**(9), 6073–6085, DOI: **10.1021/acscatal.6b01728**.

42 A. Fong, C. Vandervelden, S. L. Scott and B. Peters, Computational Support for Phillips Catalyst Initiation via Cr–C Bond Homolysis in a Chromacyclopentane Site, *ACS Catal.*, 2018, **8**(3), 1728–1733, DOI: **10.1021/acscatal.7b03724**.

43 Ø. Espelid and K. J. Børve, Molecular-Level Insight into Cr/Silica Phillips-Type Catalysts: Polymerization-Active Dinuclear Chromium Sites, *J. Catal.*, 2002, **206**(2), 331–338, DOI: **10.1006/jcat.2001.3499**.

44 A. Goodrow and A. T. Bell, A Theoretical Investigation of the Selective Oxidation of Methanol to Formaldehyde on Isolated Vanadate Species Supported on Silica, *J. Phys. Chem. C*, 2007, **111**(40), 14753–14761, DOI: **10.1021/jp072627a**.

45 J. Handzlik, R. Grybos and F. Tielens, Structure of Monomeric Chromium(VI) Oxide Species Supported on Silica: Periodic and Cluster DFT Studies, *J. Phys. Chem. C*, 2013, **117**(16), 8138–8149, DOI: **10.1021/jp3103035**.

46 A. Fiedler, D. Schröder, W. Zummack and H. Schwarz, Reversible β-Hydrogen Transfer between Fe(C2H5)+ and HFe(C2H4)+: Case of Two-State Reactivity?, *Inorg. Chim. Acta*, 1997, **259**(1–2), 227–235, DOI: **10.1016/S0020-1693(97)05450-9**.

47 Y. Sun, H. Tang, K. Chen, L. Hu, J. Yao, S. Shaik and H. Chen, Two-State Reactivity in Low-Valent Iron-Mediated C–H Activation and the Implications for Other First-Row Transition Metals, *J. Am. Chem. Soc.*, 2016, **138**(11), 3715–3730, DOI: **10.1021/jacs.5b12150**.

48 R. Gounder and E. Iglesia, The Roles of Entropy and Enthalpy in Stabilizing Ion-Pairs at Transition States in Zeolite Acid Catalysis, *Acc. Chem. Res.*, 2012, **45**(2), 229–238, DOI: **10.1021/ar200138n**.

49 R. N. Perutz, S. Sabo-Etienne and A. S. Weller, Metathesis by Partner Interchange in σ-Bond Ligands: Expanding Applications of the σ-CAM Mechanism, *Angew. Chem.*, 2022, **61**(5), e202111462, DOI: **10.1002/anie.202111462**.

50 C. A. Gaggioli, J. Sauer and L. Gagliardi, Hydrogen Atom or Proton Coupled Electron Transfer? C–H Bond Activation by Transition-Metal Oxides, *J. Am. Chem. Soc.*, 2019, **141**(37), 14603–14611, DOI: **10.1021/jacs.9b04006**.

51 J. M. Mayer, Hydrogen Atom Abstraction by Metal–Oxo Complexes: Understanding the Analogy with Organic Radical Reactions, *Acc. Chem. Res.*, 1998, **31**(8), 441–450, DOI: **10.1021/ar970171h**.